In situ Raman spectroscopic observation of polymer chains in semi-crystalline polyethylene solids

doi: 10.1515/zpc-2020-1618

In situ Raman spectroscopic observation of polymer chains in semi-crystalline polyethylene solids

Yusuke Hiejima, Takumitsu Kida and Koh-hei Nitta*

Department of Chemical and Materials Science, Kanazawa University, Kakuma Campus, Kanazawa 920-1192, Japan

Keywords: *In situ* Raman spectroscopy; Semi-crystalline polymer; Morphology; Deformation; Polyethylene

*Corresponding author: nitta@se.kanazawa-u.ac.jp. (Koh-hei Nitta)

In situ Raman spectroscopy is applied for polyethylene solid under various environments to elucidate the morphological and conformational changes. The trans conformation retains up to higher temperature for high-density polyethylene, reflecting higher stability of the orthorhombic crystals composed of stacked trans chains. It is suggested that the conversion of the non-crystalline trans chains to the crystalline phase is the microscopic origin of thermal history in the crystallinity, whereas the transformation between the trans and gauche conformers is practically in thermal equilibrium. Microscopic and dynamic mechanism of deformation during uniaxial stretching is investigated for the molecular orientation and the microscopic load sharing on the crystalline and amorphous chains. Lower crystallinity results in smoother and higher orientation toward the stretching direction, as well as higher load on the amorphous chains, during tensile elongation.

1. Introduction

Polymeric materials have been used as one of the major three materials along with metals and inorganic compounds. Excellent properties of polymers such as lightweight, flexibility, unrusting, sanitary and high designability encourage replacement from other materials. Then, more than 350 million metric tons of plastics are produced in 2018 [1], and it has been estimated that 8.3 billion metric tons of plastics have ever been produced [2]. Polyethylene (PE) and polypropylene are the major two polymers occupying approximately 50% of the total production of plastics [1].

High-density polyethylene (HDPE) is composed of long CH_2 main chains attached without or with only a small amount of pendant short CH_2 branches. Introduction of short and/or long branched chains, which leads to lower crystallinity and density, gives medium-density and low-density polyethylene (MDPE and LDPE) as softer PE [3]. Owing to its variation of the thermal and mechanical properties maintaining its chemical characteristics, PE has been used in variety of applications such as bottles, pipes and bags.

Thermoplastic polymer products are commonly formed via solidification from the melt state. During solidification, polymer chains are folded to form its crystalline structure, though appreciable portion of polymer chains remains in the amorphous region, because of entanglement of polymer chains. Consequently, lamellar structure of the crystalline and amorphous layers is spontaneously formed in semi-crystalline polymer solids. The radiating growth of lamellar crystal results in a spherulite with a diameter of several micrometers. It has been demonstrated that these supermolecular structures composed of the crystalline and amorphous chains are responsible for the mechanical properties of semi-crystalline polymers, such as Young's modulus, yield stress, strength, toughness, failure and fracture [3]. Thus, the microscopic nature and the mechanism of formation has been investigated intensively [4, 5].

Vibrational spectroscopy [6] has been used to characterize polymeric materials. Infrared absorption spectroscopy (IR) has been commonly used for investigating the microscopic structure in polymers. Raman spectroscopy, which is called as a complementary method of IR, is advantageous for polymeric systems. Vibrations of the skeletal C-C bonds in the main chains are strongly Raman active, while IR is sensitive to pendant polar groups. Raman spectroscopy can be directly applied for thick polymer molds, whereas IR measurements are restricted to the surface or thin films (typically less than 100 μm thickness). Both of these two spectroscopic methods are used to determine the molecular orientation of the crystalline and amorphous chains which strongly affect the physical properties of polymeric materials [7]. While IR gives the orientation function as the averaged value, polarized Raman spectroscopy enable us to visualize the distribution of molecular orientation [8]. While the orientation behavior can be also detected by X-ray diffraction and

birefringence measurements, nevertheless, these vibrational spectroscopies are suitable for investigating microscopic environment of polymer chains such as microscopic load sharing and conformation of the molecular chains. It should be emphasized that *in situ* measurements are crucially important for polymeric materials, because the internal structure of polymeric materials dynamically changes in accordance with the temporal changes of the external field owing to their elastic nature. For example, supermolecular structure undergoes appreciable structural relaxation after the removal of the applied external stress.

In this work, the application of *in situ* Raman spectroscopy on PE under various conditions is described with the analyses and interpretations for the spectral changes. It is demonstrated that *in situ* Raman spectroscopy is a powerful tool to elucidate the microscopic mechanism of polymer chains under various environments.

2. Experimental

2.1 Sample preparation and characterization

The PE pellets supplied by Tosoh Corporation (Tokyo, Japan) were compression molded to form an isotropic sheet with a thickness of approximately 1 mm by the following procedure. The pellets were melted and compressed in a hot press at 210°C and 20 MPa for 5 min followed by quenching in an iced water. The test specimens were cut out from the sample sheet. Square (2 mm×2 mm) and double-notched (the width of 4 mm and gauge length of 2 mm) specimens were used for heating/cooling and uniaxial stretching experiments, respectively.

Differential scanning calorimetry (DSC) measurements were conducted under a nitrogen atmosphere at a heating/cooling rate of ±2 °C/min with a PerkinElmer Diamond DSC. The volumetric crystallinity (χ_v) was determined by the Archimedes method by assuming the density of the crystalline and amorphous phases (ρ_c =1000, ρ_a=855 [kg/m^3] [9]).

2.2 *In situ* Raman spectroscopy

A diode-pumped solid-state laser (RLK-640-200, LASOS) at a wavelength of 640 nm and a power of 200 mW was used as the excitation light. The laser light was irradiated on the central portion of the test specimen. A small tensile tester and a hot stage (F-82, Mettler Toledo) was installed for *in situ* measurements under uniaxial stretching and heating/cooling process, respectively. It is noteworthy that the tensile tester is equipped with a double drawing mechanism to maintain the center of the specimen at the same position. The scattered light was collimated by a pair of convex lenses into a monochromator attached to a charge-coupled device (CCD) camera (SpectraPro 2300i and PIXIS 100, Princeton instruments). A laser-line filter (LD01-640/8-12.5, Semrock) was inserted to purify the excitation light, and a long-pass filter (BLP01-635R-50, Semrock) was used to block the Rayleigh scattering from the sample. For polarized Raman spectroscopy, a half-wavelength plate and a wire-grid polarizing plate were inserted for the polarizer and the analyzer, respectively. Each Raman spectra was accumulated for 10 times with an exposure time of 1 s.

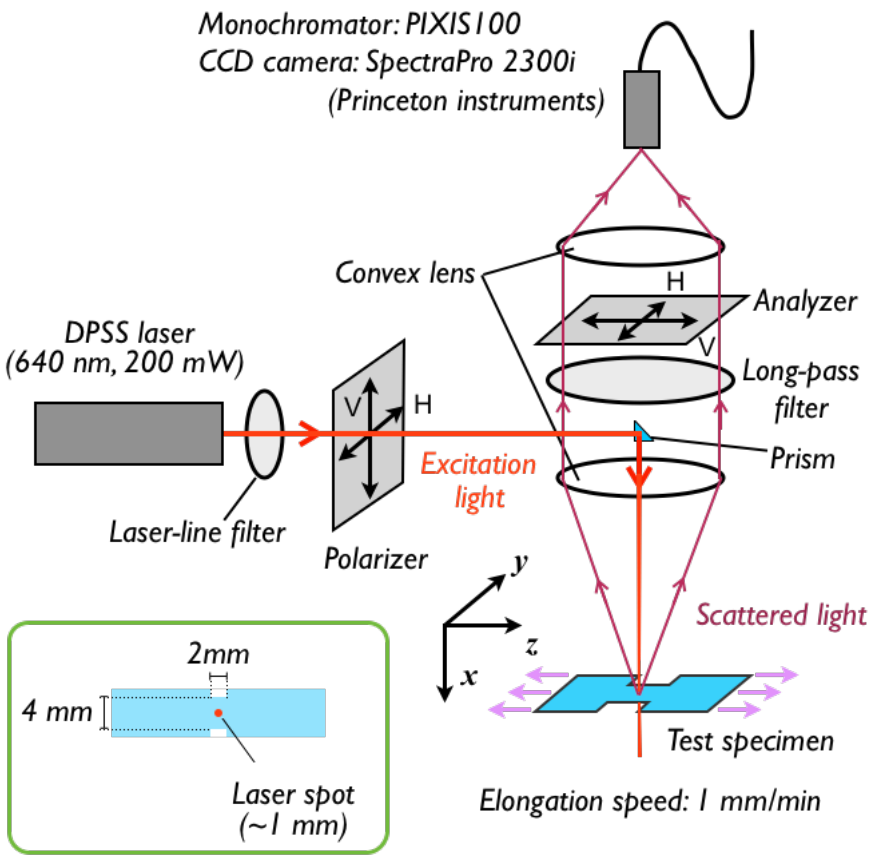

Fig. 1 Optical setup for *in situ* Raman spectroscopy during tensile test. The sample geometry of the test specimen for tensile tests is also shown.

2.3 Raman spectral analysis

2.3.1 Morphology

The assignments for the Raman bands of PE are shown in Tables 1. The fraction of the trans sequence and amorphous chains are described as [10-13]

$$\chi_{\mathrm{t}} = \frac{I_{1298}}{I_{1298} + I_{1305}}, \tag{1}$$

$$\chi_{\mathrm{a}} = \frac{I_{1305}}{I_{1298} + I_{1305}}. \tag{2}$$

The orthorhombic crystallinity is given as [11]

$$\chi_{\mathrm{c}} = \frac{I_{1418}}{A(I_{1298} + I_{1305})}, \tag{3}$$

where A=0.46 is an experimental constant. Note that the sum of the intensities of 1298 and 1305 cm^{-1} is known to be independent of temperature so that the sum of the intensities of these two bands can be used as an internal standard [11]. For PE, it has been reported that the trans conformers are located not only in the crystalline region but also in the amorphous region. The trans chains in the amorphous region are usually interpreted as the intermediate component, which has been detected by NMR [14-16] and Raman [17] spectroscopies. Since the crystalline phase is solely comprised with trans chains, the fraction of the non-crystalline consecutive trans (NCCT) chains are given by [12]

$$\chi_{\mathrm{NCCT}} = \chi_{\mathrm{t}} - \chi_{\mathrm{c}}. \tag{4}$$

According to the calculation for the assignments for the C–C stretching modes for PE, the Raman bands at 1063 and 1130 cm^{-1} are attributed to the long trans sequences with more than 11 trans bonds [10, 18]. Thus, the fraction of long trans sequence is determined as

$$\chi_{\mathrm{LT}} = \frac{I_{1130}}{A'(I_{1298} + I_{1305})}, \tag{5}$$

where A'=0.80 is an experimentally-determined constant [19].

Table 1 Assignments for Raman bands of PE [10, 20-23]

Peak position /cm^{-1}	Vibrational mode [a)]	Phase
1063	ν_{as} (C-C)	Long trans sequence (n>11)
1080	ν (C-C)	Amorphous
1130	ν_{s} (C-C)	Long trans sequence (n>11)
1298	τ (CH_2)	Trans sequence
1305	τ (CH_2)	Amorphous
1418	δ (CH_2) + ω (CH_2)	Crystalline (orthorhombic)
1440	δ (CH_2)	Amorphous trans
1460	δ (CH_2)	Amorphous

[a)] ν: stretching, ν_{as}: anti-symmetric stretching, ν_{s}: symmetric stretching, τ: twisting, δ: bending, ω: wagging

2.3.2 Peak shift

It has been demonstrated that vibrational modes of polymers show appreciable peak shift under the microscopic stress on the molecular chains, because the force constant of the molecular vibration is affected by the applied stress owing to anharmonicity of oscillation [24-27]. The C-C stretching modes of PE show red and blue shifts under stretching and compressive stress, respectively. The peak shift $\Delta\nu$ due to stretching is written as

$$\Delta\nu = \nu(\varepsilon) - \nu(0), \tag{6}$$

where $\nu(\varepsilon)$ and $\nu(0)$ are the peak positions of a Raman band at the strains of ε and 0, respectively. It has been demonstrated that the peak shift is proportional to the applied stress σ in the absence of plastic deformation [26, 28].

$$\Delta\nu = \alpha\sigma \tag{7}$$

Here the peak shift coefficient α is constant for each vibrational mode (e.g. α=–5.0 and –3.8 cm^{-1}/GPa for the 1063 and 1130 cm^{-1} bands of PE [29], respectively).

2.3.3 Molecular orientation

The orientation distribution function, which is a probability distribution function of polymer chains oriented at an Euler angle (θ, η, ϕ) is written as [30, 31]

$$N(\theta,\eta,\phi) = \sum_{l=0}^{\infty}\sum_{m=-l}^{l}\sum_{n=-l}^{l} W_{lmn} Z_{lmn}(\cos\theta) e^{-im\eta} e^{-in\phi}, \tag{8}$$

where $Z_{lmn}(\xi)$ is the generalized Legendre function. Under cylindrical symmetry, eq.(8) can be simplified to a Legendre expansion as [32]

$$N(\theta) = \sum_{l=0}^{\infty}\left(\frac{2l+1}{2}\right)\langle P_l\rangle P_l(\cos\theta), \tag{9}$$

where $P_l(x)$ (l=2,4,6,...) is the l-th Legendre polynomial and θ is the polar angle from the stretching direction. The l-th moment $\langle P_l\rangle$ is written as

$$\langle P_l\rangle = \int_0^{\pi} N(\theta) P_l(\cos\theta)\sin\theta d\theta. \tag{10}$$

The second moment $\langle P_2\rangle$, which represents the average polar angle has been commonly used for evaluation of orientation. For example, random orientation gives $\langle P_2\rangle$=0, and the complete orientation in parallel and perpendicular to stretching direction is represented by $\langle P_2\rangle$=1 and –0.5, respectively. While infrared (IR) spectroscopy gives only $\langle P_2\rangle$, higher rank parameters are obtained by various spectroscopic techniques; Raman and nuclear magnetic resonance (NMR) spectroscopies provide up to l=4 and 8, respectively, and X-ray diffraction gives every $\langle P_l\rangle$ in principle [33].

Polarized Raman spectra can be obtained by controlling the polarization geometry by a pair of polarizers. Rigorous theory has been developed by Bower [32, 34], and a simplified and practical model has been developed by Frisk *et al* [35]. According to the Frisk's depolarized model, the intensity of polarized Raman signal and the orientation parameters are related as follows.

$$I_{vv} = b\left(\frac{8a^2+4a+3}{15} + 2\langle P_2\rangle\frac{4a^2-a-3}{21} + 3\langle P_4\rangle\frac{a^2-2a+1}{35}\right), \tag{11}$$

$$I_{hh} = b\left(\frac{8a^2+4a+3}{15} - 4\langle P_2\rangle\frac{4a^2-a-3}{21} + 8\langle P_4\rangle\frac{a^2-2a+1}{35}\right), \tag{12}$$

$$I_{vh} = b\left(\frac{a^2-2a+1}{15} + \langle P_2\rangle\frac{a^2-2a+1}{21} - 4\langle P_4\rangle\frac{a^2-2a+1}{35}\right), \tag{13}$$

where I_{ij} is the intensity of a Raman band with A_g symmetry (the 1130 cm^{-1} band for PE), and the i and j represent the polarization direction (v or h) of the polarizer and analyzer, respectively. The constant a is a function of the principal value of the Raman tensor, and the constant b depends on the instruments and sample. For unstretched specimens, we can set $\langle P_2\rangle$=$\langle P_4\rangle$=0. Thus, the polarization ratio is given as

$$\frac{I_{vh}}{I_{hh}} = \frac{a^2-2a+1}{8a^2+4a+3}. \tag{14}$$

If we assume that the depolarization ratio remains constant during deformation, the value of a is obtained by eqn. (14). Then, we can determine the orientation parameters $\langle P_2\rangle$ and $\langle P_4\rangle$ at given strains by combining eqns. (11)-(13) [35].

The combination of $\langle P_2\rangle$ and $\langle P_4\rangle$ enable us to describe the probability distribution of the molecular orientation, because contribution by the higher-rank terms can be included by the maximum entropy method [32, 36]. The most-probable orientation distribution function is determined by maximizing the information entropy of the molecular orientation.

$$S = -\int_0^\pi N(\theta)\ln N(\theta)d\theta \tag{15}$$

The most-probable orientation distribution function is written as [8, 36-39]

$$N_{\mathrm{mp}}(\theta) = \frac{\exp\left[\lambda_2 P_2(\cos\theta) + \lambda_4 P_4(\cos\theta)\right]}{\displaystyle\int_0^\pi \exp\left[\lambda_2 P_2(\cos\theta) + \lambda_4 P_4(\cos\theta)\right]\sin\theta d\theta}, \tag{16}$$

where λ_2 and λ_4 are the Lagrange multipliers determined by the following constraints.

$$\int_0^\pi N_{\mathrm{mp}}(\theta)\sin\theta d\theta = 1 \tag{17}$$

$$\int_0^\pi P_2(\cos\theta)N_{\mathrm{mp}}(\theta)\sin\theta d\theta = \langle P_2\rangle \tag{18}$$

$$\int_0^\pi P_4(\cos\theta)N_{\mathrm{mp}}(\theta)\sin\theta d\theta = \langle P_4\rangle \tag{19}$$

The most-probable value of $\langle P_4\rangle$ under a given value of $\langle P_2\rangle$, which is also determined by the maximum entropy method, is approximately represented by [37]

$$\langle P_4\rangle_{\mathrm{mp}} = -0.083\langle P_2\rangle + 1.366\langle P_2\rangle^2 - 1.899\langle P_2\rangle^3 + 1.616\langle P_2\rangle^4 \tag{20}$$

for positive $\langle P_2\rangle$, and

$$\langle P_4\rangle_{\mathrm{mp}} = 0.052\langle P_2\rangle + 1.574\langle P_2\rangle^2 + 3.968\langle P_2\rangle^3 + 8.057\langle P_2\rangle^4 \tag{21}$$

for negative $\langle P_2\rangle$.

3. Results and discussion

3.1.1 *In situ* Raman spectra during heating

In situ Raman spectra of HDPE (M_w=1.0×10^5, M_w/M_n=5.9) and LDPE (M_w=6.9×10^4, M_w/M_n=3.8) during heating are shown in Fig. 2. In the solid phase, Raman spectra of HDPE and LDPE have several sharp peaks assigned to long trans sequence mainly residing in the crystalline layer. At the melting point (T_m=132°C for HDPE and 104°C for LDPE), these sharp peaks disappear and, three broad amorphous bands are observed in the melt state. It is noteworthy that the amorphous Raman bands at 1080 and 1305 cm^{-1} are observed as small and broad peaks next to the crystalline counterpart in the solid phase.

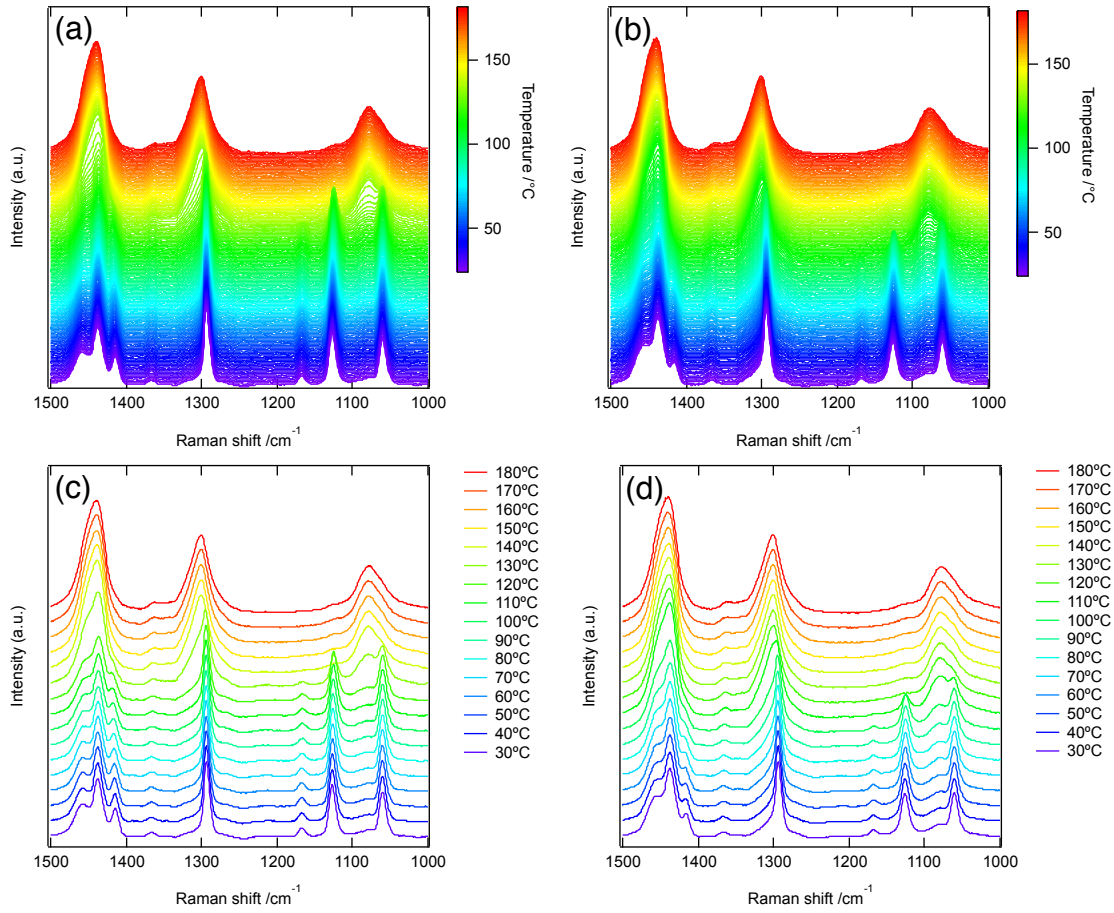

Fig. 2 *In situ* Raman spectra of (a,c) HDPE and (b,d) LDPE at various temperatures (a,b) shown by the color scale and (c,d) at selected temperatures during heating.

3.1.2 Morphological changes during heating and cooling

The mass fractions of various conformers are plotted against temperature in Fig. 3. For HDPE, the crystallinity gradually decreases with increasing temperature, followed by a sharp decrease at ~120°C. It has been demonstrated that various motions in the crystalline chains are activated in the α relaxation region; the intercrystalline motions are activated above ~60°C, and the intracrystalline motions are also activated above ~120°C [40]. The fraction of NCCT chain shows gradual increase above ~60°C, whereas the fraction of the trans sequence remains at the same level. Since expansion of the interchain distance in orthorhombic PE crystal is observed above ~60°C [41, 42], the decrease of crystallinity complemented by the increase of NCCT chains is explained that the orthorhombic crystalline regularity is lost by the interchain expansion maintaining trans conformation. Similar phenomenon has been reported for *n*-paraffins that the orthorhombic crystalline phase is transformed into the quasi hexagonal phase (rotator phase) consisting of the trans sequence owing to thermal expansion of the interchain distance [43]. The decrease of crystallinity in the vicinity of the melting temperature (T_m=132°C) is accompanied by a sharp drop of the fraction of the trans sequence, suggesting that the conformation is significantly disordered owing to activation of the intracrystalline motions. While the crystallinity drops to zero at the melting point, the trans sequences persist even above the melting temperature for 2-3°C.

As shown in Fig. 3(b), the crystallinity of LDPE is markedly smaller than that of HDPE, and it rapidly decreases with increasing temperature, indicating poor stability of the crystalline structure. The fraction of trans sequence is also appreciably smaller with steeper slope than that of HDPE, suggesting that conformational disorder persists even at room temperature. Then, it is suggested that the branched chains of LDPE prefer mixture of trans and gauche conformers rather than consecutive trans chains. Considering that the existence of long chain branches hinders the formation of stacked trans sequence (crystallization) and the thickening of lamellar crystal, thin and unstable lamellar crystals in LDPE are prone to be melted even at low temperatures.

While hysteresis is clearly observed for the crystallinity during heating and cooling, it is obscured for the trans sequence as shown in Fig. 4. These results suggest that the transformation between trans and gauche conformers are practically in thermal equilibrium, and the thermal history is originated in nano scale segregation, i.e. morphology, and/or intermediate phase.

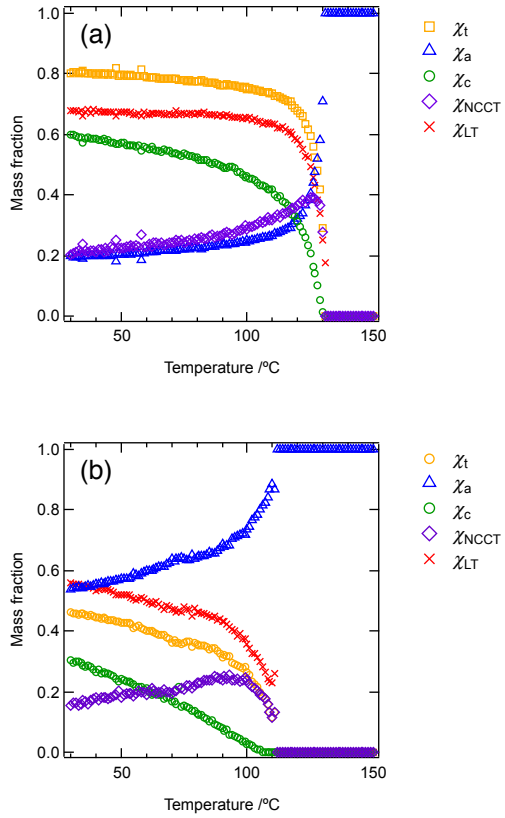

Fig. 3 Temperature dependence of fractions of various conformers for (a) HDPE and (b) LDPE.

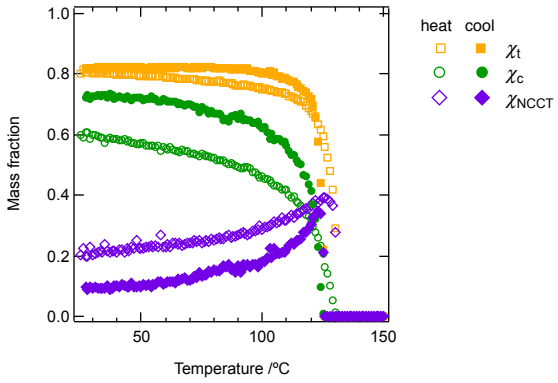

Fig. 4 Temperature dependence of fraction of conformers during heating (open) and cooling (closed) for HDPE.

3.2 Deformation during uniaxial stretching

3.2.1 Stress-strain curve

The stress-strain curves of HDPE (M_w=1.7×10^5, M_w/M_n=15, χ_v =0.58), MDPE (M_w=1.7×10^5, M_w/M_n=15, χ_v=0.54) and LDPE (M_w=6.9×10^4, M_w/M_n=3.8, χ_v=0.45) are shown in Fig. 5. At small strains, the stress linearly increases in accordance with the Hooke's law (elastic region). For HDPE and MDPE, the stress shows a maximum at $\varepsilon \approx 0.6$ (first yield point), followed by a drop accompanied by a small shoulder at $\varepsilon \approx 1$ (second yield point). In the yielding region, the lamellar crystals are fragmented into smaller lamellar blocks followed by the reorientation into the stretching direction, which leads to the catastrophic transition from the spherulitic to the fibrillar structures [44, 45]. Beyond the yielding region, the fibrillar structure composed of the highly-oriented crystals is formed so that the stress resumes increasing in the strain-hardening region. For LDPE whose stress level is appreciably smaller than that of HDPE and MDPE, the first yield point is observed as a shoulder at $\varepsilon \approx 0.8$, and the second yield point is more pronounced at $\varepsilon \approx 2$.

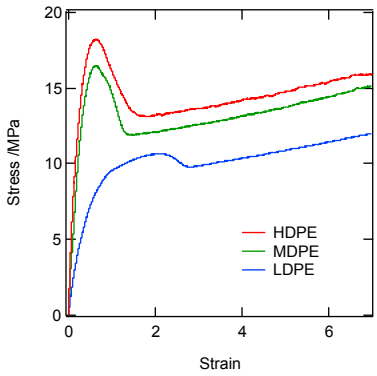

Fig. 5 Stress-strain curves for HDPE, MDPE and LDPE.

3.2.2 *In situ* Raman spectra during tensile test

In situ polarized Raman spectra of HDPE and LDPE at various strains under uniaxial stretching are shown in Fig. 6. The Raman spectra show obvious changes during elongation. The intensity of the 1130 cm^{-1} band increases with increasing the strain, whereas that of the 1063 cm^{-1} band remains practically at the same level. This is a consequence of the molecular orientation of PE chains. The 1130 cm^{-1} band is sensitive to orientation, because its Raman tensor has A_g symmetry, whereas the 1063 cm^{-1} (in B_{2g}+B_{3g} symmetry) is practically independent of orientation. It is noteworthy that the 1130 cm^{-1} band is used to determine orientation parameters of PE. Elimination of the 1418 cm^{-1} band at high strains is explained by disordering of orthorhombic crystalline lattice [46, 47].

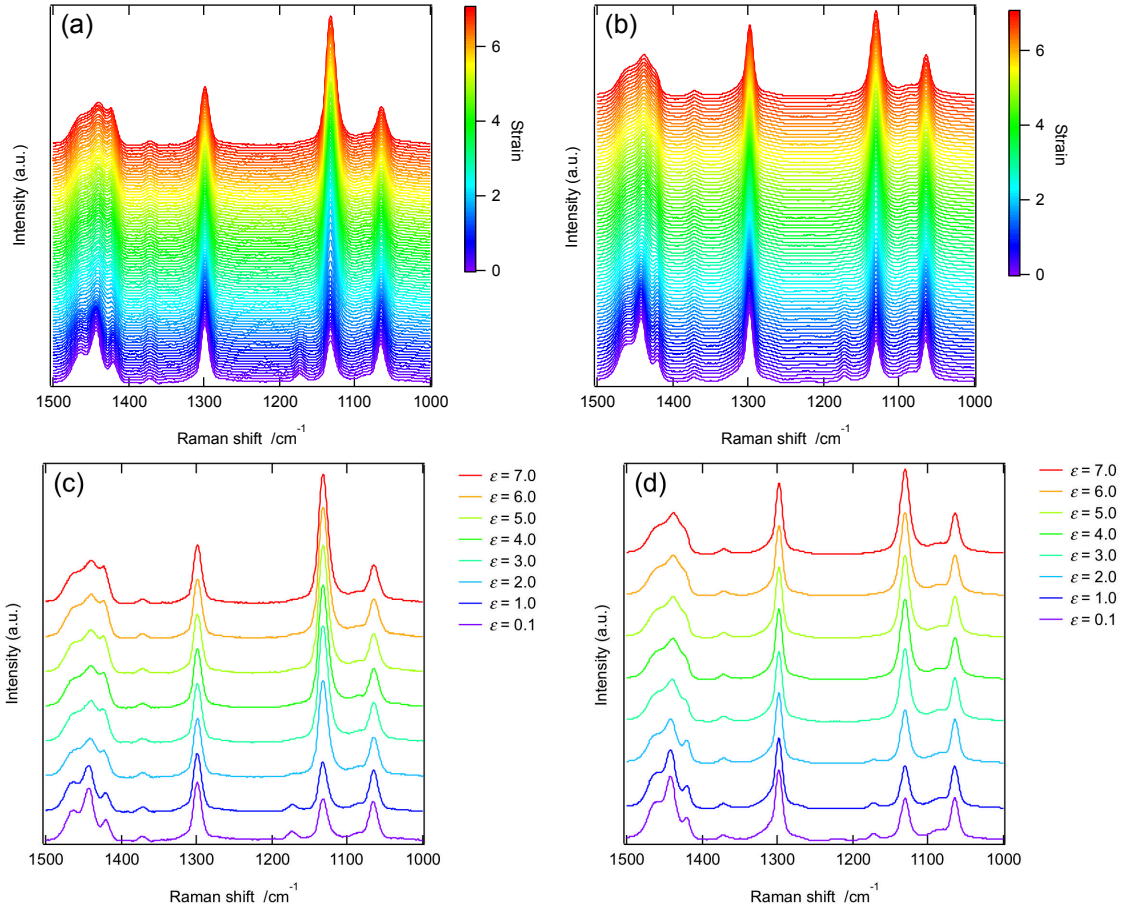

Fig. 6 *In situ* Raman spectra of (a,c) HDPE and (b,d) LDPE at various strains (a,b) shown by the color scale and (c,d) at selected strains during uniaxial stretching.

3.2.3 Orientation of crystalline chains

The strain dependence of the orientation parameters of trans sequence is shown along with the stress-strain curve in Fig. 7. In the elastic region, both of $\langle P_2 \rangle$ and $\langle P_4 \rangle$ remains practically zero, indicating that the specimen remains unoriented. Beyond the first yield point, $\langle P_2 \rangle$ shows a step-wise increase, whereas $\langle P_4 \rangle$ shows a drop for HDPE. The increase of $\langle P_2 \rangle$ is a consequence of molecular orientation toward the stretching direction, which is visualized by the orientation distribution function in Fig. 8. The drop of $\langle P_4 \rangle$ in the yielding region of HDPE gives tilted orientation at $\theta \approx 40°$, as observed in the orientation distribution function ($\varepsilon \approx 2$, in Fig. 8(a)). The tilted orientation is explained by steric hindrance of densely-packed rigid and bulky lamellar cluster units [48] which are formed by fragmentation of lamellar crystals during yielding [49, 50]. Except for the yielding region of HDPE, the value of $\langle P_4 \rangle$ is practically reproduced by the most-probable value ($\langle P_4 \rangle_{mp}$) calculated by eqn. (20), indicating that the molecular orientation of PE is essentially represented by simple uniaxial orientation to the stretching direction. These orientation behavior is commonly observed for HDPE, while the HDPE with wider molecular weight distribution shows higher orientation [51]. It is interesting to note that biaxial orientation along and perpendicular to the stretching direction is observed for the PE gels which is a blend of liquid paraffin and PE resin [52]. Besides the disappearance of the tilted orientation in the yielding region, lower crystallinity gives higher orientation at high strains for MDPE and LDPE, suggesting smooth orientation into the stretching direction. Similar orientation behavior is observed for HDPE at elevated temperatures [53].

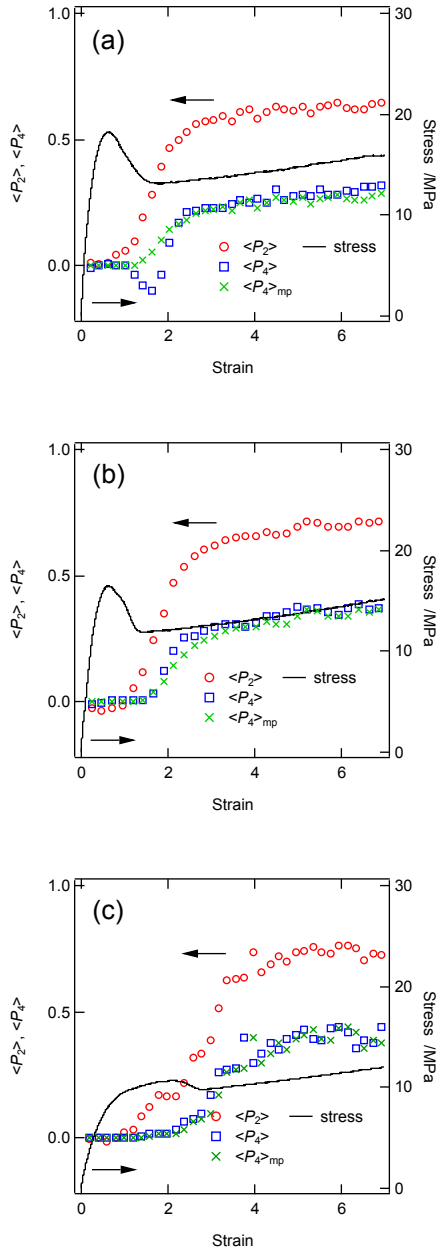

Fig. 7 Strain dependence of orientation parameters along with the stress-strain curves for HDPE, MDPE and LDPE.

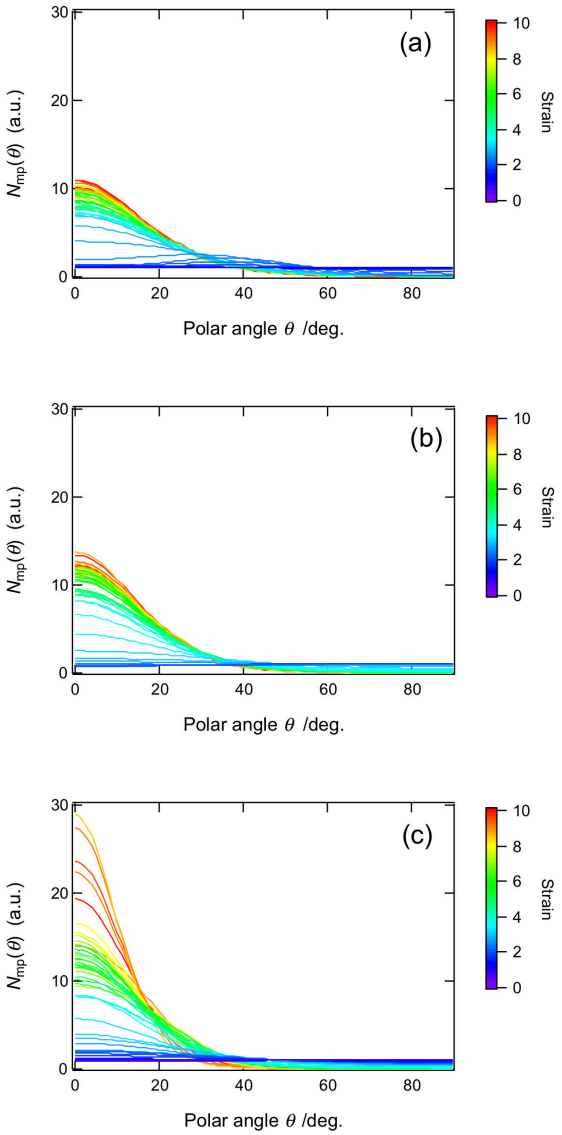

Fig. 8 Most-probable orientation distribution functions at various strains (shown by the color scale) for (a) HDPE, (b) MDPE and (c) LDPE.

3.2.4 Load sharing on crystalline and amorphous chains

The peak shifts for the crystalline chains during uniaxial stretching are shown along with the stress-strain curve in Fig. 9. The 1063 cm^{-1} band shows gradual red shift beyond the first yield point, indicating that stretching load is applied along the polymer chain. For HDPEs, the 1130 cm^{-1} band shows a blue shift in the yielding region, indicating compression stress perpendicular to the polymer chain. On the other hand, the peak shift of the 1130 cm^{-1} band for LDPE remains almost constant in the yielding region. Considering that HDPE shows an obvious narrowing in width of the specimens (necking) in the yielding region, the compression load applied on the crystalline chains for HDPE is caused by the contraction perpendicular to stretching direction (Poisson's contraction). Both of the 1063 and 1130 cm^{-1} bands show red shifts in the strain-hardening region, and the red shift increases with the crystallinity. Because the peak shift coefficient is constant for each Raman band, the larger red shift is explained that larger stress is loaded on the crystalline chains. The red and blue shifts for the 1418 cm^{-1} band are the consequences of contraction and expansion of the interchain distance [46, 47], respectively. The slight contraction in the yielding region owing to compression stress is followed by a pronounced expansion of the crystalline lattice, suggesting distortion of the crystalline structure caused by the fragmentation of the lamellar crystals at the yielding region, which is also observed by X-ray diffraction [41].

The peak shifts for the amorphous chains are shown in Fig. 10. The amorphous band at 1460 cm^{-1} shows blue shift in the yielding region of HDPE, followed by a gradual decrease to zero. The amorphous trans band at 1440 cm^{-1} shows similar behavior, but slightly lower values. Considering that taut-tie chains, which are the amorphous trans chains connecting the adjacent lamellar crystals, act as the stress transmitters of the applied stress on the specimen, the red shift of the 1440 cm^{-1} band from the 1460 cm^{-1} is explained by preferential stretching load on taut-tie chains. For HDPE, both amorphous bands show blue shifts in the yielding region as well as the crystalline bands, suggesting that the compression load owing to the Poisson's contraction is homogeneously applied on the crystalline and amorphous chains. On the other hand, for LDPE in Fig. 10(d), the compression stress in the yielding region vanishes and the stretching stress on the amorphous chains is markedly enhanced. The larger stress on the amorphous chains is consistent with lower stress on the crystalline chains, as observed in Fig. 9. It is noteworthy that large peak shift owing to enhanced stress on the amorphous chains is also observed for elastomeric materials such as ultra-low density polyethylene [54]. It should be emphasized that vibrational spectroscopy is more sensitive to such dynamical effects on polymer chains during deformation than other techniques such as *in situ* X-ray measurements [55].

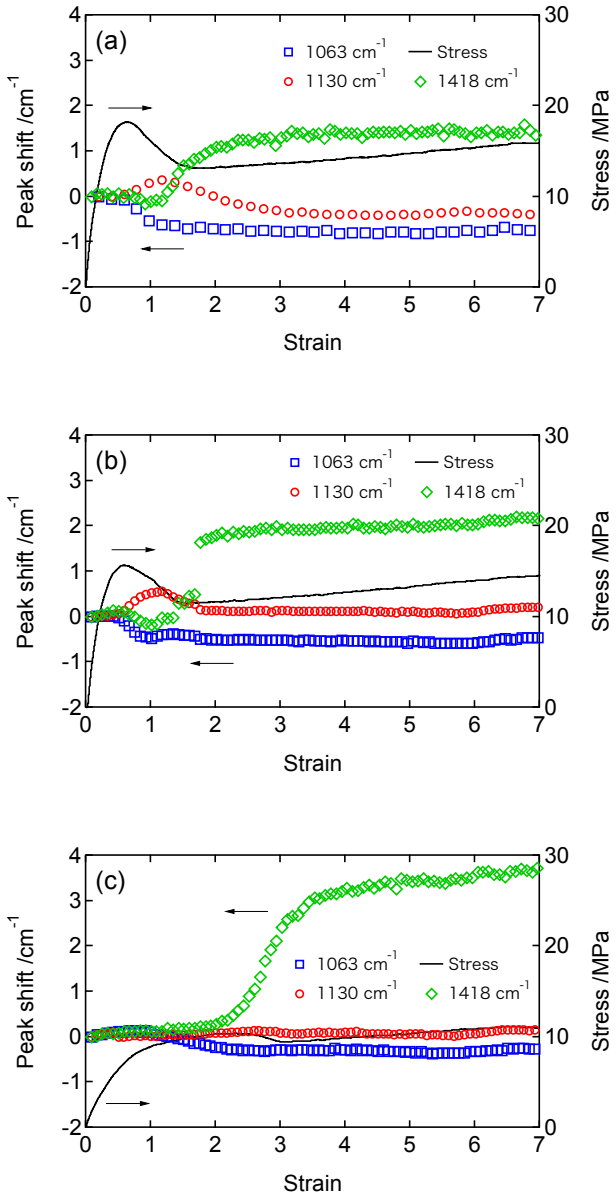

Fig. 9 Strain dependence of the peak shifts of the crystalline chains at 1063 (squares),1130 (circles) and 1418 (diamonds) cm^{-1} along with the stress-strain curves for (a) HDPE, (b) MDPE and (c) LDPE.

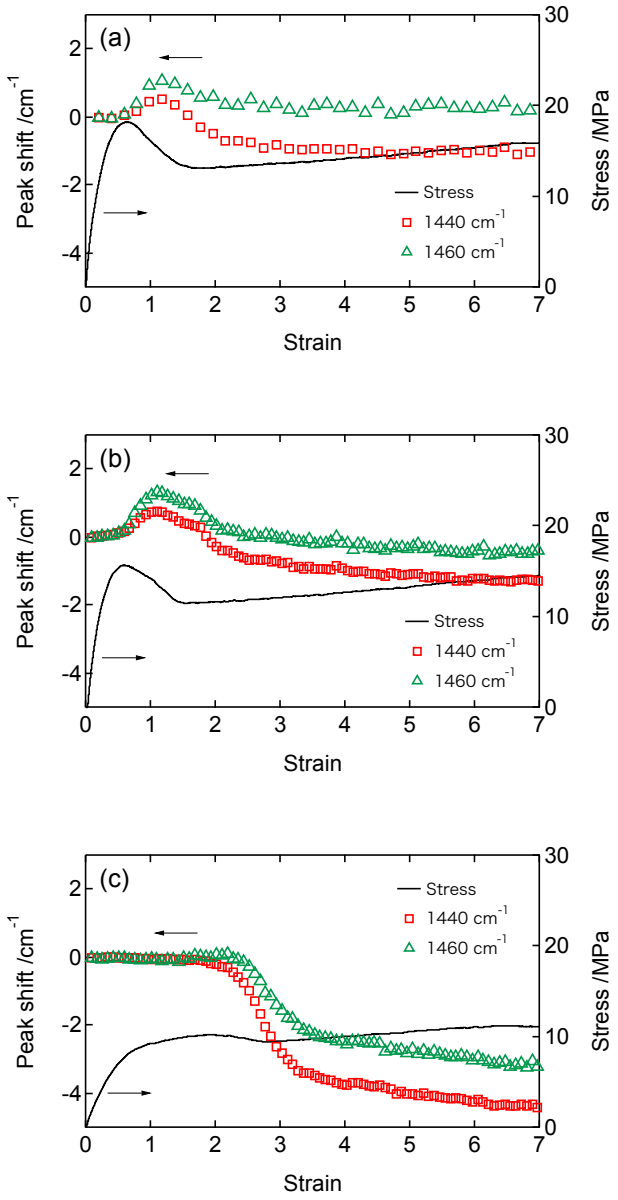

Fig. 10 Strain dependence of the peak shifts of the amorphous chains at 1440 (squares) and 1460 (triangles) cm^{-1} along with stress-strain curves for (a) HDPE, (b) MDPE and (c) LDPE.

4. Concluding remarks

The present work demonstrated that *in situ* Raman spectroscopy is a powerful tool to elucidate microscopic structural changes of polyethylene under various conditions. The morphological changes with temperature such as the slight disordering of the orthorhombic crystalline regularity were successfully detected, and these phenomena were explained by the conformational changes. The microscopic deformation mechanism such as molecular orientation and load sharing was elucidated. The present method has also been applied for other polymeric systems, such as morphology [56, 57] and orientation [58, 59] for polypropylene. Considering the flexibility of Raman spectroscopy, the combination with Raman microscope and/or the application under extreme conditions (e.g. at high pressures) would provide physical insights on the fundamental nature of polymeric materials.

Reference

1. PlasticsEurope: Plastics – the Facts 2019 An analysis of European plastics production, demand and waste data. (2019).
2. Geyer, R., Jambeck, J.R., Law, K.L.: Production, use, and fate of all plastics ever made. Science Advances. 3, e1700782 (2017).
3. Ward, I.M., Sweeney, J.: Mechanical Properties of Solid Polymers. Wiley (2013).
4. Young, R.J., Lovell, P.A.: Introduction to polymers. CRC Press (2011).
5. Strobl, G.R.: The Physics of Polymers: Cencepts for Understanding Their Structures and Behavior. Springer (2007).
6. Bower, D.I., Maddams, W.F.: The Vibrational Spectroscopy of Polymers. Cambridge University Press (1992).
7. Ward, I.M. ed: Structure and Properties of Oriented Polymers. Chapman and Hall (1997).
8. Tanaka, M., Young, R.J.: Review Polarised Raman spectroscopy for the study of molecular orientation distributions in polymers. J. Mater. Sci. 41, 963–991 (2006).
9. Brandrup, J., Immergut, E.H., Grulke, E.A., Abe, A., Bloch, D.R.: Polymer handbook. Wiley (1999).
10. Meier, R.J.: Studying the length of trans conformational sequences in polyethylene using Raman spectroscopy: a computational study. Polymer. 43, 517–522 (2002).
11. Strobl, G.R., Hagedorn, W.: Raman spectroscopic method for determining the crystallinity of polyethylene. J. Polym. Sci. Polym. Phys. Ed. 16, 1181–1193 (1978).
12. Migler, K.B., Kotula, A.P., Walker, A.R.H.: Trans-Rich Structures in Early Stage Crystallization of Polyethylene. Macromolecules. 48, 4555–4561 (2015).
13. Hiejima, Y., Kida, T., Takeda, K., Igarashi, T., Nitta, K.-H.: Microscopic structural changes during photodegradation of low-density polyethylene detected by Raman spectroscopy. Polym. Degrad. Stab. 150, 67–72 (2018).
14. Bergmann, K., Nawotki, K.: Eine neue Interpretation der Breitlinien-Kernresonanzspektren von linearem Polyäthylen. Colloid. Polym. Sci. 219, 132–144 (1967).
15. Kitamaru, R., Horii, F., Hyon, S.H.: Proton magnetic resonance studies of the phase structure of bulk-crystallized linear polyethylene. J. Polym. Sci. Polym. Phys. Ed. 15, 821–836 (1977).
16. Kitamaru, R., Horii, F.: NMR approach to the phase structure of linear polyethylene. In: Polymer Chemistry. pp. 137–178. Springer (1978).
17. Strobl, G.R., Hagedorn, W.: Raman spectroscopic method for determining the crystallinity of polyethylene. J. Polym. Sci. Polym. Phys. Ed. 16, 1181–1193 (1978).
18. Koglin, E., MEIER, R.J.: Conformational dependence of Raman frequencies and intensities in alkanes and polyethylene. Comput. Theor. Polym. Sci.. 9, 327–333 (1999).
19. Lagaron, J.M., Dixon, N.M., Reed, W., Pastor, J.M., KIP, B.J.: Morphological characterisation of the crystalline structure of cold-drawn HDPE used as a model material for the environmental stress cracking (ESC) phenomenon. Polymer. 40, 2569–2586 (1999).
20. Gall, M.J., Hendra, P.J., Peacock, C.J., Cudby, M.E.A., Willis, H.A.: Laser-Raman spectrum of polyethylene: Part 1. Structure and analysis of the polymer. Polymer. 13, 104–108 (1972).
21. Gall, M.J., Hendra, P.J., Peacock, O.J., Cudby, M.E.A., Willis, H.A.: The laser-Raman spectrum of polyethylene. Spectrochim. Acta A: Mol. Spectrosc. 28, 1485–1496 (1972).
22. Bailey, R.T., Hyde, A.J., Kim, J.J., McLeish, J.: Raman studies on oriented, high modulus, polyethylene. Spectrochim. Acta A: Mol. Spectrosc. 33, 1053–1058 (1977).
23. Schachtschneider, J.H., Snyder, R.G.: Vibrational analysis of the n-paraffins—II. Spectrochim. Acta. 19, 117–168 (1963).
24. Wool, R.P.: Infrared studies of deformation in semicrystalline polymers. Polym. Eng. Sci. 20, 805–815 (1980).
25. Wool, R.P.: Measurements of infrared frequency shifts in stressed polymers. J. Polym. Sci. Polym. Phys. Ed. 19, 449–457 (1981).
26. Tashiro, K., Wu, G., Kobayashi, M.: Quasiharmonic treatment of infrared and raman vibrational frequency shifts induced by tensile deformation of polymer chains. J. Polym. Sci. Part B: Polym. Phys. 28, 2527–2553 (1990).
27. Tashiro, K., Minami, S., Wu, G., Kobayashi, M.: Quasiharmonic treatment of infrared and raman vibrational frequency shifts induced by tensile deformation of polymer chains. II. Application to the polyoxymethylene and isotactic polypropylene single chains and the three-dimensional orthorhombic polyethylene crystal. J. Polym. Sci. Part B: Polym. Phys. 30, 1143–1155 (1992).

28. Kida, T., Hiejima, Y., Nitta, K.-H.: Raman Spectroscopic Study of High-density Polyethylene during Tensile Deformation. Int. J. Experim. Spectrosc. Tech. 1, 1–6 (2016).
29. Tashiro, K., Wu, G., Kobayashi, M.: Morphological effect on the Raman frequency shift induced by tensile stress applied to crystalline polyoxymethylene and polyethylene: spectroscopic support for the idea of an inhomogeneous stress distribution in polymer material. Polymer. 29, 1768–1778 (1988).
30. Roe, R.-J.: Description of Crystallite Orientation in Polycrystalline Materials. III. General Solution to Pole Figure Inversion. J. Appl. Phys. 36, 2024–2031 (1965).
31. Roe, R.-J.: Methods of description of orientation in polymers. J. Polym. Sci. A-2 Polym. Phys. 8, 1187–1194 (1970).
32. Bower, D.I.: Orientation distribution functions for uniaxially oriented polymers. J. Polym. Sci. Polym. Phys. Ed. 19, 93–107 (1981).
33. Kawai H., Nomura S.: Characterisation and Assessment of Polymer Orientation. In: Developments in Polymer Characterisation—4. pp.211-263. Springer (1983).
34. Bower, D.I.: Investigation of molecular orientation distributions by polarized raman scattering and polarized fluorescence. J. Polym. Sci. Polym. Phys. Ed. 10, 2135–2153 (1972).
35. Frisk, S., Ikeda, R.M., Chase, D.B., Rabolt, J.F.: Determination of the molecular orientation of poly(propylene terephthalate) fibers using polarized Raman spectroscopy: a comparison of methods. Appl. Spectrosc. 58, 279–286 (2004).
36. Berne, B.J.: Molecular Reorientation in Liquids and Gases. J. Chem. Phys. 49, 3125 (1968).
37. Pottel, H., Herreman, W., van der Meer, B.W., Ameloot, M.: On the significance of the fourth-rank orientational order parameter of fluorophores in membranes. Chem. Phys. Lett. 102, 37–44 (1986).
38. Labarthet, F.L., Buffeteau, T., Sourisseau, C.: Orientation Distribution Functions in Uniaxial Systems Centered Perpendicularly to a Constraint Direction. Appl. Spectrosc. 54, 699–705 (2000).
39. Tanaka, M., Young, R.J.: Molecular orientation distributions in the crystalline and amorphous regions of uniaxially oriented isotactic polypropylene films determined by polarized Raman spectroscopy. J. Macromol. Sci. B. B44, 967–991 (2005).
40. Nakayasu, H., Markovitz, H., Plazek, D.J.: The Frequency and Temperature Dependence of the Dynamic Mechanical Properties of a High Density Polyethylene. Trans. Soc. Rheol. 5, 261–283 (1961).
41. Wang, Z., Liu, Y., Liu, C., Yang, J., Li, L.: Understanding structure-mechanics relationship of high density polyethylene based on stress induced lattice distortion. Polymer. 160, 170–180 (2019).
42. Bärenwald, R., Goerlitz, S., Godehardt, R., Osichow, A., Tong, Q., Krumova, M., Mecking, S., Saalwächter, K.: Local flips and chain motion in polyethylene crystallites: A comparison of melt-crystallized samples, reactor powders, and nanocrystals. Macromolecules. 47, 5163–5173 (2014).
43. Sirota, E.B., King, H.E., Jr, Singer, D.M., Shao, H.H.: Rotator phases of the normal alkanes: An x-ray scattering study. J. Chem. Phys. 98, 5809–5824 (1998).
44. Nitta, K.-H., Takayanagi, M.: Tensile yield of isotactic polypropylene in terms of a lamellar-cluster model. J. Polym. Sci. Part B: Polym. Phys. 38, 1037–1044 (2000).
45. Nitta, K.-H., Takayanagi, M.: Novel Proposal of Lamellar Clustering Process for Elucidation of Tensile Yield Behavior of Linear Polyethylenes. J. Macromol. Sci. B. 42, 107–126 (2003).
46. Otegui, J., Vega, J.F., Martín, S., Cruz, V., Flores, A., Domingo, C., Martínez-Salazar, J.: The unit cell expansion of branched polyethylene as detected by Raman spectroscopy: an experimental and simulation approach. J. Mater. Sci. 42, 1046–1049 (2007).
47. Lagaron, J.M.: On the use of a Raman spectroscopy band to asses the crystalline lateral packing in polyethylene. J. Mater. Sci. 37, 4101–4107 (2002).
48. Kida, T., Oku, T., Hiejima, Y., Nitta, K.-H.: Deformation mechanism of high-density polyethylene probed by in situ Raman spectroscopy. Polymer. 58, 88–95 (2015).
49. Kuriyagawa, M., Nitta, K.-H.: Structural explanation on natural draw ratio of metallocene-catalyzed high density polyethylene. Polymer. 52, 3469–3477 (2011).
50. Nitta, K.-H., Kuriyagawa, M.: Application of catastrophe theory to neck initiation of metallocene-catalyzed high-density polyethylene. Polym. J. 44, 245–251 (2011).
51. Kida, T., Hiejima, Y., Nitta, K.-H.: Rheo-Raman Spectroscopic Study on Uniaxial Deformation Behavior of High-Density Polyethylene Solids with Various Molecular Weight Distributions. Macromolecules. 52, 4590–4600 (2019).
52. Hiejima, Y., Okuda, T., Kono, K., Nitta, K.-H.: Orientation behavior and deformation mechanism of polyethylene gels during cold drawing determined by in situ Raman spectroscopy. Polymer. 176, 30–37 (2019).
53. Kida, T., Hiejima, Y., Nitta, K.-H.: Rheo-optical Raman study of microscopic deformation in high-density polyethylene under hot drawing. Polym Test. 44, 30–36 (2015).
54. Kida, T., Hiejima, Y., Nitta, K.-H.: Rheo-Raman spectroscopic study of microscopic deformation behavior for ultra-low-density polyethylene. Polym. Int. 67, 1335–1340 (2018).
55. Xiong, B., Lame, O., Chenal, J.-M., Rochas, C., Seguela, R., Vigier, G.: Amorphous Phase Modulus and Micro–Macro Scale Relationship in Polyethylene via in SituSAXS and WAXS. Macromolecules. 48, 2149–2160 (2015).
56. Khafagy, R.M.: In situ FT-Raman spectroscopic study of the conformational changes occurring in isotactic polypropylene during its melting and crystallization processes. J. Polym. Sci. Part B: Polym. Phys. 44, 2173–2182 (2006).
57. Hiejima, Y., Takeda, K., Nitta, K.-H.: Investigation of the Molecular Mechanisms of Melting and Crystallization of Isotactic Polypropylene by in Situ Raman Spectroscopy. Macromolecules. 50, 5867–5876 (2017).
58. Kida, T., Hiejima, Y., Nitta, K.H.: Molecular orientation behavior of isotactic polypropylene under uniaxial stretching by rheo-Raman spectroscopy. Express Polym. Lett. 10, 701–709 (2016).

59. Kida, T., Hiejima, Y., Nitta, K.-H.: Rheo-Raman Study of Isotactic Polypropylene Under Tensile Deformation. Macromol. Symp. 377, 1700019–5 (2018).